EUROPEAN HEMATOLOGY ASSOCIATION
haematologica
Journal of the European Hematology Association

Human RAD52 – a novel player in DNA repair in cancer and immunodeficiency

by Sujal Ghosh, Andrea Hönscheid, Gregor Dückers, Sebastian Ginzel, Holger Gohlke, Michael Gombert, Bettina Kempkes, Wolfram Klapper, Michaela Kuhlen, Hans-Jürgen Laws, René Martin Linka, Roland Meisel, Christian Mielke, Tim Niehues, Detlev Schindler, Dominik Schneider, Friedhelm R Schuster, Carsten Speckmann, and Arndt Borkhardt

Haematologica 2016 [Epub ahead of print]

Citation: Ghosh S, Hönscheid A, Dückers G, Ginzel S, Gohlke H, Gombert M, Kempkes B, Klapper W, Kuhlen M, Laws HJ, Linka RM, Meisel R, Mielke C, Niehues T, Schindler D, Schneider D, Schuster FR, Speckmann C, and Borkhardt A. Human RAD52 – a novel player in DNA repair in cancer and immunodeficiency. Haematologica. 2016; 101:xxx doi:10.3324/haematol.2016.155838

Human RAD52 – a novel player in DNA repair in cancer and immunodeficiency

Sujal Ghosh[1,2], Andrea Hönscheid[1], Gregor Dückers[3], Sebastian Ginzel[1], Holger Gohlke[4], Michael Gombert[1], Bettina Kempkes[5], Wolfram Klapper[6], Michaela Kuhlen[1], Hans-Jürgen Laws[1], René Martin Linka[1], Roland Meisel[1], Christian Mielke[7], Tim Niehues[3], Detlev Schindler[8], Dominik Schneider[9], Friedhelm R Schuster[1], Carsten Speckmann[10], Arndt Borkhardt[1]

1 Department of Pediatric Oncology, Hematology and Clinical Immunology, Medical Faculty, Center of Child and Adolescent Health, Heinrich-Heine-University, Düsseldorf, Germany
2 Infection, Immunity, Inflammation, Molecular and Cellular Immunology Section, UCL Great Ormond Street Institute of Child Health, London, UK
3 Department of Pediatrics, Helios Hospital Krefeld, Krefeld, Germany
4 Institute for Pharmaceutical and Medicinal Chemistry, Heinrich-Heine-University, Düsseldorf, Germany
5 Department of Gene Vectors, Helmholtz Center Munich, German Research Center for Environmental Health, Munich, Germany
6 Department of Pathology, Haematopathology Section and Lymph Node Registry, University Medical Centre Schleswig-Holstein, Kiel, Germany
7 Institute of Clinical Chemistry and Laboratory Diagnostics; Medical Faculty, Heinrich-Heine-University, Düsseldorf, Germany
8 Institute for Human Genetics, University of Würzburg, Germany
9 Clinic of Pediatrics, Municipal Hospital Dortmund, Dortmund, Germany
10 Centre for Chronic Immunodeficiency (CCI) and Centre of Pediatrics, University of Freiburg, Freiburg, Germany

Corresponding author:

Dr. Sujal Ghosh, MD

Department of Pediatric Oncology, Hematology and Clinical Immunology

Medical Faculty, Center of Child and Adolescent Health, Heinrich-Heine-University

Moorenstraße 5, 40225 Duesseldorf, Germany

Telephone: +49-211 811-8297

Telefax: +49-211 811-6539

Mail to: sujal.ghosh@med.uni-duesseldorf.de

Exposure to mutagenic sources such as ionizing radiation or chemical agents leads to damage of the genome, however DNA double-strand breaks (DSB) and the subsequent repair machinery pose a basic necessity for a functional immune response [1].

Two pathways restore genomic integrity: Non-homologous end-joining (NHEJ) is error-prone and leads to TCR and immunoglobulin diversity; defects in the NHEJ process result in severe combined immunodeficiency, radiosensitivity and developmental errors [2].

On the other hand homologous recombination (HR) conveys a high-fidelity process. It is restricted to the S and G2 phase as a homologous "sister chromatid" template is required. HR is vital in providing repair to DSB and DNA interstrand crosslinks (ICL) [3]. ICL are toxic DNA lesions preventing separation of the two complementary double helix strands. Chemotherapeutic agents as mitomycin C (MMC), nitrogen mustards and platinum compounds, can induce irreversible covalent linkage [1]. Fanconi anemia (FA) is an autosomal-recessive disorder due to a mutation in one of at least 18 genes leading to bone marrow failure, developmental delay and increased incidence of malignancies [4]. The inability to repair ICL is a key feature of all FA genes. *BRCA2* (=*FANCD1*) and other genes involved in breast and ovarian cancer also show regulation on ICL repair [5]. We report on an 18-year-old man with profound combined immunodeficiency, Epstein-Barr-Virus (EBV) lymphoproliferation and chemosensitivity similar to FA patients and a missense mutation in the *RAD52* gene. While *RAD51*, its paralog *RAD51C*, *BRCA1*, *BRCA2* and *PALB2* have been associated with FA and DNA damage repair; the precise function of RAD52 in the recombination process is still unclear. We suspect a modification in the ssDNA annealing function of the protein and hence a disturbed homologous recombination leading to cancer and lymphoproliferation in the patient and his family. The patient presented with leukopenia with predominantly reduced lymphocytes (absent B, CD4 and CD8 T cells, expansion of

TCRγδ cells). Candidate primary immunodeficiencies (PIDs) were ruled out by various immunological investigations. Immunohistochemistry of an extracted lymph node revealed polymorphic monoclonal EBV-associated B cell lymphoproliferation of type III latency (Fig. S1 - detailed history see supplemental). The patient´s mother died early from breast carcinoma (age of 39) and further cases of colon carcinoma had been reported in the maternal lineage. We performed whole-exome-sequencing on peripheral blood of the patient, the patient´s sister and father, and stored samples of the deceased patient´s mother, which revealed 122 single nucleotide variants (SNV) common in the patient and the mother. Three were in PID genes (*BCL10*, *CHD7* and *PRF1*), which were excluded due to the clinical presentation. Only one SNV came to our attention as we saw a connection to a known DNA repair pathway. Interestingly, our in-house tool to detect SNV near known PID genes also highlighted the same SNV to be related to known PID with DNA repair disorders (Fig. S2). Both, patient and his mother showed a heterozygous missense mutation in *RAD52* (c.547C>T, P183S) in the ssDNA-annealing domain of the protein (Fig. S3), confirmed by capillary sequencing. *BRCA1/2* analysis in the mother did not show any abnormalities. We did not find any de-novo mutations in a known or likely PID-causing gene.

Molecular dynamic (MD) simulations were performed to compare the average structure of wild type (wt) *RAD52* with the mutant one. We depicted the influence of the P183S mutation on dynamics and structure (Fig. 1). As expected for a proline->serine substitution, we demonstrated a change in configuration and increase in distance between the C_α atom of residue 183 and the close α4` helix. Average structures of both protein variants are highly structurally similar, indicating only a local influence of the P183S mutation. However, structural changes triggered by the P183S mutation caused reorientation of a K169 sidechain subsequently, which were predicted to disturb ssDNA binding and, hence, the ssDNA

annealing function of RAD52 (detailed analysis in supplemental). Primary human fibroblasts were exposed to MMC, a known DNA intercalating agent, and cultured for 48h as part of our diagnostic strategy in patients with unknown cytopenia. Cells, exposed to MMC showed an increased number of G2 phase cells, indicating that cells were in a cycle arrest after damage by MMC. A G2 increase was not seen in healthy controls, but detected in a similar quantity in an internal control with fibroblasts from an MMC sensitive disease control (Fig. 2A). Lymphoblastoid cell lines (LCL) from patient´s bone marrow were analyzed in a routine flow cytometric cellular DNA content analysis, showing repeatedly abnormal aneuploid DNA content (Fig. 2B).

SsDNA binding of purified mutant P183S and wt protein was assessed in an electrophoretic mobility shift assay (EMSA). The P183S-ssDNA complexes showed an increased mobility shift in repeated experiments, although densitometric analyses of EMSA bands revealed a lower amount of complex formation in the P183S-ssDNA bands despite an increasing protein concentration (Fig 3A,B). Similar changes (as the Y171A variant) have been seen in other publications [6].

We transfected HT-1080 cells with wt EGFP-RAD52 and EGFP-RAD52^{P183S} via bicistronic expression vectors previously used for stable expression in human cells. We assayed the ability of the P183S variant and wt to produce DNA breaks detectable as RAD52 foci by immunofluorescence in transfected HT1080 cells. The cells were irradiated with 1 Gy or 10 Gy, and cultured for 4h or 24 hours respectively. While all conditions showed a numerically decreased foci formation in the P183S cell line, the higher (10 Gy) irradiation and longer (24 hours) culture period showed a further, but non-significant, decrease in the mutant (Fig. 3C,D). RAD51 foci after MMC induction were counted previously in patient's primary

fibroblasts showing no abnormalities (data not shown), thus we did not repeat that assay in EGFP-RAD52^{P183S} transfected cells.

In conclusion, we describe a patient with T cell depletion associated comorbidities as EBV lymphoproliferation and severe varicella infection. The past medical history suggests a combined immunodeficiency. The patient presented to us with hypersplenism, hence WBC was low and the patient´s immunological phenotype could not be revealed completely. The most striking abnormality was the detection of FA-like chemosensitivity in patient`s fibroblasts. The overlap of genes involved in breast cancer and FA [7] and increased mortality due to adenocarcinoma in the maternal lineage led us to the assumption of an inherited disease or at least variant conferring a higher risk of disease.

The discovery of FA genes has revealed the molecular pathway (FA/*BRCA*) of DNA maintenance. The core element is E3 ligase-mediated monoubiquitination of the protein complex D2-I, which is carried out by an upstream complex consisting of classical FA proteins. Downstream of this step other proteins associate with the D2-I complex and apply HR to the induced DSB. Proteins involved in this part of the FA/*BRCA* pathway have a major role in HR and vice versa [8]. RAD52, which was not associated with this pathway in humans, exists in an undecameric ring structure and consists of an N-terminal ssDNA annealing, central RPA interacting and C-terminal RAD51 mediating domain [9]. Initial findings suggested an indispensable role in yeast, but increasing evidence attributes RAD52 to HR in mammalian cells. During DSB repair DNA strand exchange takes place in which a template strand invades a homologous DNA strand. RAD51 recombinase binds to replication protein A(RPA)-coated ssDNA to form a nucleoprotein filament able to invade duplex DNA. Assembly of this filament is mediated by RAD52. After capture of the second end of the DSB and strand extension RAD52 anneals RPA-coated ssDNA [6, 9-11]. The heterozygous P183S mutation

lies in the ssDNA-annealing domain and our assays suggest that ssDNA annealing of mutant P183S is impaired. A second DNA binding site was identified in RAD52 for dsDNA and showed that impaired ability to form RAD52-ssDNA leads to a less stable complex with dsDNA, which leads further to decreased HR [6]. We show evidence of some reduced formation of RAD52 foci in the P183S-transfected HT1080 cell line after irradiation suggesting reduced capacity of HR. Furthermore the MMC assay indicates disturbance of ICL repair, of which HR plays a major role. Synthetic lethality of RAD52 inactivation in BRCA1, BRCA2 and PALB2 deficient cells has been described suggesting RAD52 as part of an alternative repair pathway parallel to RAD51 mediated HR [12, 13]. We and other groups propose the alternative *RAD52* pathway as being required for DNA stability and attribute a tumor-suppressor function. Additive germline mutations in other DNA repair genes might confer an increased tumor risk. We are aware of the possible interaction of RAD52 with genes of NHEJ (*LIG4* or MRN complex genes), as also depicted in our gene-association network. However due to full aplasia when we investigated the patient, we could not check for NHEJ related disturbance (e.g. TCR repertoire). We observe a heterozygous mutation in the patient and mother with reduced mRNA expression and suggestive assays for reduced HR capacity. In line with emerging data in genome wide association studies in other patients with malignancies, results from targeted synthetic lethality studies and our own findings in reduced RAD52 foci and ssDNA annealing we strongly suggest that *RAD52* plays a major role in DNA repair and cancer predisposition.

1. Muniandy PA, Liu J, Majumdar A, Liu ST, Seidman MM. DNA interstrand crosslink repair in mammalian cells: step by step. Crit Rev Biochem Mol Biol. 2010;45(1):23-49.

2. Woodbine L, Gennery AR, Jeggo PA. The clinical impact of deficiency in DNA non-homologous end-joining. DNA Repair. 2014;16:84-96.

3. San Filippo J, Sung P, Klein H. Mechanism of eukaryotic homologous recombination. Annu Rev Biochem. 2008;77:229-257.

4. Ameziane N, May P, Haitjema A, et al. A novel Fanconi anaemia subtype associated with a dominant-negative mutation in RAD51. Nat Commun. 2015;6:8829.

5. Hussain S, Wilson JB, Medhurst AL, et al. Direct interaction of FANCD2 with BRCA2 in DNA damage response pathways. Hum Mol Genet. 2004;13(12):1241-1248.

6. Kagawa W, Kagawa A, Saito K, et al. Identification of a second DNA binding site in the human Rad52 protein. J Biol Chem. 2008;283(35):24264-24273.

7. Levy-Lahad E. Fanconi anemia and breast cancer susceptibility meet again. Nat Genet. 2010;42(5):368-369.

8. Longerich S, Li J, Xiong Y, Sung P, Kupfer GM. Stress and DNA repair biology of the Fanconi anemia pathway. Blood. 2014;124(18):2812-2819.

9. Lok BH, Powell SN. Molecular pathways: understanding the role of Rad52 in homologous recombination for therapeutic advancement. Clin Cancer Res. 2012;18(23):6400-6406.

10. McIlwraith MJ, West SC. DNA repair synthesis facilitates RAD52-mediated second-end capture during DSB repair. Mol Cell. 2008;29(4):510-516.

11. Gaines WA, Godin SK, Kabbinavar FF, et al. Promotion of presynaptic filament assembly by the ensemble of S. cerevisiae Rad51 paralogues with Rad52. Nat Commun. 2015;6:7834.

12. Feng Z, Scott SP, Bussen W, et al. Rad52 inactivation is synthetically lethal with BRCA2 deficiency. Proc Natl Acad Sci U S A. 2011;108(2):686-691.

13. Lok BH, Carley AC, Tchang B, Powell SN. RAD52 inactivation is synthetically lethal with deficiencies in BRCA1 and PALB2 in addition to BRCA2 through RAD51-mediated homologous recombination. Oncogene. 2013;32(30):3552-3558.

Manuscript figure legend of "Human RAD52 – a novel player in DNA repair in cancer and immunodeficiency"

Figure 1 – Overall structural similarity of wild type and mutant RAD52 (A) Overlay of average structures of wild type RAD52 (colored by a gradient from blue to red) and the S183 mutant (white). The average structures were obtained from MD simulations of 80 ns length; the proteins are depicted in cartoon representation. The average structures differ by a C_α atom rmsd of 1.0 Å (B) As in panel A), but rotated by 90° (C) Local influence of the P183S mutation on dynamics and structure. Cutaway of the RAD52 11mer (white), with one protomer colored in dark grey. The orange region depicts helix α4, the preceding region of 3_{10} helices, and part of the loop between α4 and α5 where the largest changes in rmsf are observed between wild type and mutant RAD52. The backbone atoms of residue 183 are depicted as spheres. Helix α4' of the neighboring protomer is colored blue. The distance measured between the C_α atom of residue 183 and the center of α4' is shown as a dotted black line. The side chain of K169 is shown in stick representation. The distance measured between atom C_γ of P183 or O_γ of S183 and N_z of K169, respectively, is indicated by a dotted-dashed line. The orientation of the sidechain of K169 was determined with respect to the center of the 11mer (red cross). The dashed arc indicates the position of ssDNA according to suggestions (Kagawa et al, 2002)

Figure 2 – (A) Mitomycin C (MMC) sensitivity assay - patient fibroblasts (without MMC, left chart) were exposed to MMC (12 ng/ml) and cultured for 48h. Staining with DAPI shows an increased number of G2 phase cells, indicating that cells are in a cycle arrest after induced damage by MMC, a known DNA intercalating agent (second right chart). A G2 increase is not

seen in healthy controls (second left chart), but detected in a similar quantity in an internal control with fibroblasts from a MMC sensitive patient control (right chart). Cell cycle distribution among mentioned samples – chi-square test show significant difference between healthy control and patient sample and MMC sensitive patient control, while there is no difference between patient sample and MMC sensitive patient control (bottom right chart) **(B)** Flow cytometric DNA content measurement of two different LCLs generated from patient´s bone marrow stained with PI following ethanol fixation. Both cell lines were cultured and processed under same standard conditions from the same specimen. Left: Patient LCL#1 cells (blue) show slightly increased DNA amount than normal control LCLs (grey). Right: Patient LCL#2 cells (green) show aneuploidy (another experiment polyploidy), compared to healthy human samples.

Figure 3 – (A) Electrophoretic mobility shift assay (EMSA) of wild type and mutant synthetic RAD52 protein (0,1-1 µM) complexes which were formed with a 50bp ssDNA. The purified mutant protein forms faster migrating complexes compared to wt, despite **(B)** densitometric analyses of EMSA bands for wt and mutant RAD52/ssDNA complexes reveal a lower amount of complex formation irrespective of applied protein concentration in the mutant. Data are representative of three independent experiments. **(C)** Representative examples of HT-1080 cells stably expressing GFP-RAD52 or GFP-RAD52^{P183S}after irradiation with 10 Gy and further 24 hours of culture. Phase contrast and fluorescence microscopy. **(D)** Foci counting per cell in both cell clines after 10 Gy and 4h or 24h of subsequent culture. Irradiation with 1 Gy did not show any difference (not shown).

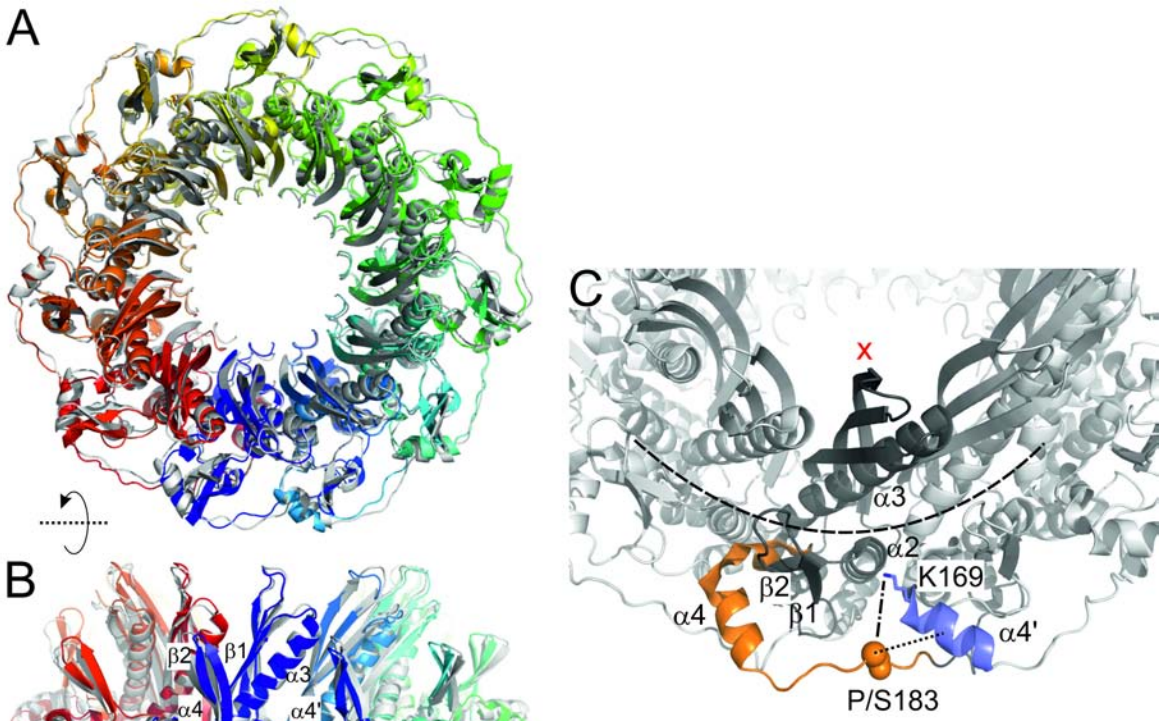
A
B
β2
β1
α3
α4
α4'
α2
C
X
α3
α2
β2
β1
K169
α4
α4'
P/S183

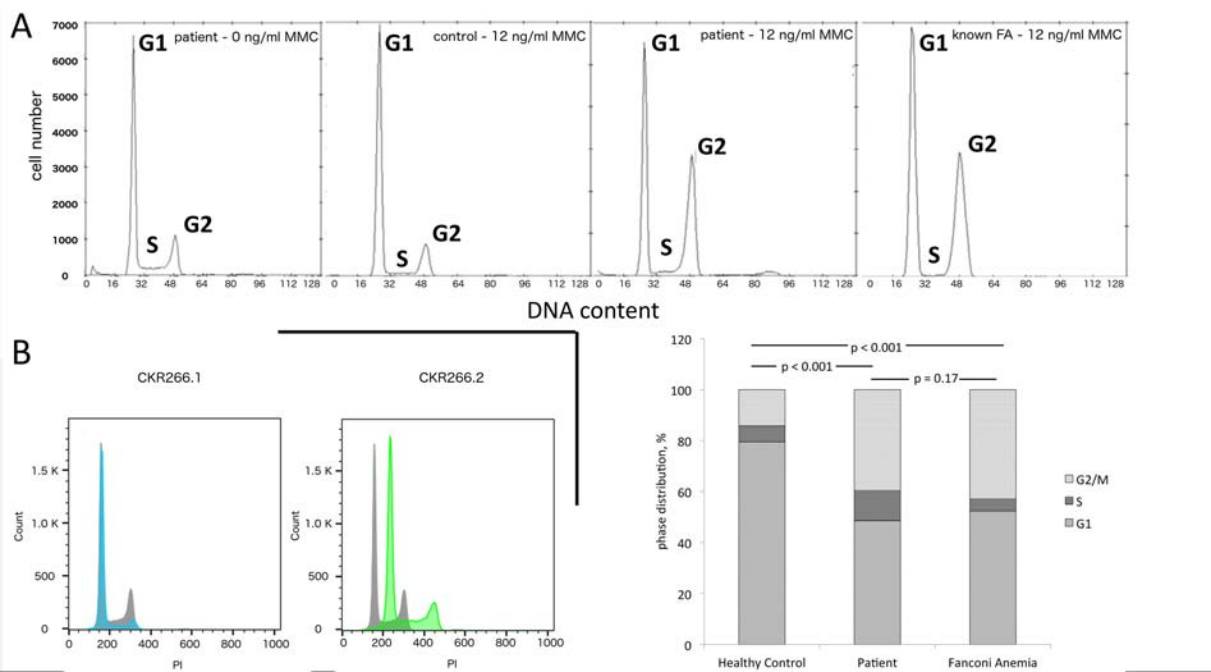
A
G1
patient - 0 ng/ml MMC
control - 12 ng/ml MMC
patient - 12 ng/ml MMC
known FA - 12 ng/ml MMC
S
G2
cell number
DNA content
B
CKR266.1
CKR266.2
Count
PI
p < 0.001
p < 0.001
p = 0.17
phase distribution, %
G2/M
S
G1
Healthy Control
Patient
Fanconi Anemia

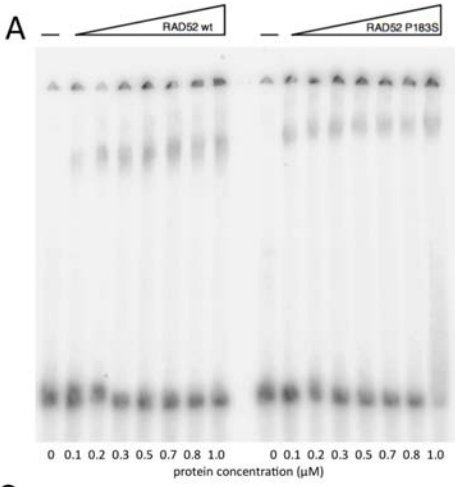
A
RAD52 wt
RAD52 P183S
0 0.1 0.2 0.3 0.5 0.7 0.8 1.0
0 0.1 0.2 0.3 0.5 0.7 0.8 1.0
protein concentration (μM)

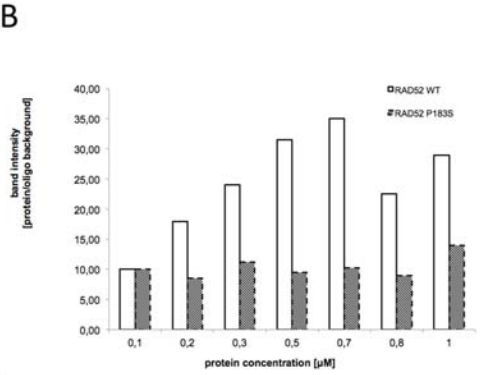
B
band intensity
[protein/oligo background]
40,00
35,00
30,00
25,00
20,00
15,00
10,00
5,00
0,00
RAD52 WT
RAD52 P183S
0,1
0,2
0,3
0,5
0,7
0,8
1
protein concentration [μM]

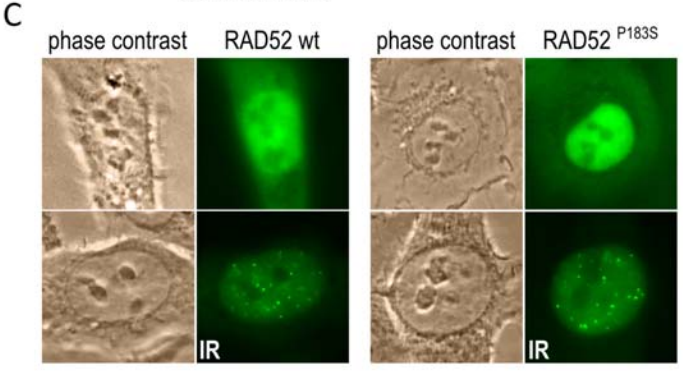
C
phase contrast
RAD52 wt
phase contrast
RAD52 P183S
IR
IR

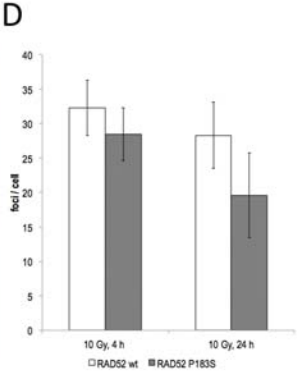
D
foci / cell
40
35
30
25
20
15
10
5
0
10 Gy, 4 h
10 Gy, 24 h
RAD52 wt
RAD52 P183S

Supplemental to "Human RAD52 – a novel player in DNA repair in cancer and immunodeficiency"

Case report

We report on an 18-year-old man, who presented at our department with chemosensitive combined immunodeficiency, EBV lymphoproliferation, severe varicella infection and vasculitis. The patient was from a non-consanguineous German background. Briefly, he suffered from recurrent respiratory tract infections (pneumonia, bronchitis and bronchiectasis) and splenomegaly since birth; at the age of five years he developed severe generalized warts (verrucae vulgares), at the age of eight years he suffered from bacterial meningitis. There were no syndromic features in the patient. Lab results revealed mild hemolytic anemia, leukopenia and reduced IgG2 and IgG4 levels. However, due to loss to follow-up a diagnosis was not established. Nine years later, he was referred to us for further evaluation as symptoms had worsened. He was suffering from varicella zoster virus meningitis and B symptoms (fever, drenching night sweat, weight loss). Hematological studies showed leukopenia with predominantly reduced lymphocytes (WBC 1200 cells/ul, Lymphocytes 6%, Absolute: CD3 20 cells/ul, CD4 5 cells/ul, CD8 1 cells/ul, CD3 γ δ 15 cells/ul, CD20 7 cells/ul, CD3-DR = absent B, CD4 and CD8 T cells, relative expansion of γδ T cells) and decreased IgG2 and IgG4 levels. As the immunological phenotype indicated a combined immunodeficiency we excluded the most obvious ones: ADA and PNP enzymatic levels were physiological, flow cytometry showed normal expression of WASP, XIAP and SAP, furthermore VDJ recombination on fibroblasts and capillary sequencing of *RAG1/2* were normal. Determination of telomere lengths was not

suggestive of dyskeratosis congenita or other telomeropathies. PCR analysis of the peripheral blood revealed low EBV viremia. The young man developed a severe herpes zoster rash at different sites; furthermore lesions resembling vasculitis were seen on lower limbs (Fig. S4). As bone marrow studies showed a normal differentiation, we attributed hypersplenism as the main cause of aplasia; splenectomy was performed (Fig. S5); within one day the white blood count (WBC) increased from aplasia to a count of more than 1000 cells/µl; however we only observed neutrophil reconstitution with continuously decreased lymphocytes. Biopsy of a left inguinal lymph node at the same time revealed polymorphic monoclonal EBV associated B cell lymphoproliferation (Fig. S1); and a chest CT demarked infiltration of the lower right lung. We treated with 4 cycles of Rituximab (375mg/m2/week); due to persistent lymphopenia and severity of the viral infections we proceeded to perform HSCT with peripheral blood stem cells from the patient's haploidentical sister (8/10 match in graft-versus-host direction, 6/10 match in host-versus-graft direction). In light of the assumed DNA repair disorder we chose a reduced-intensity conditioning regimen consisting of fludarabine (4x40 mg/m^2, days -7 to -4), thiotepa (1x8 mg/kg, day -3) and melphalan (2x50 mg/m^2, day -2), TBI (2x2 Gy, day -1) and serotherapy with ATG (3x10 mg/kg, days -10 to -8). The graft was TCRαβ/CD19 depleted before transplantation (5,3x10^6 CD34+cells/kg; 19x10^3 TCRα/β cells/kg); graft-versus-host-disease (GvHD) prophylaxis consisted of mycophenolate mofetil. The peritransplant period was uneventful. We did not observe severe infections, toxicity or GvHD. Granulocyte-Colony Stimulating Factor (G-CSF) was given from day 4, and neutrophil engraftment was achieved on day 7. Bone marrow aspiration on day 28 showed a normal marrow with 99.3% donor cells.

Methods

Patient and cell lines

Whole exome sequencing (WES) was done on peripheral blood of the patient, the patient´s sister and father, and stored samples of the deceased patient´s mother. Informed consent was obtained from the patient, the patient´s sister and father. Informed consent to analyze the sample of the deceased patient´s mother was obtained from the only children (patient and his sister) and the sister of the mother. All investigations were conducted in accordance to the Declaration of Helsinki. Patient's fibroblasts were grown from skin explant, obtained during insertion of a Hickman line. B lymphocytes from bone marrow samples were transformed for the generation of an EBV lymphoblastoid cell line (LCL) – culture conditions available upon request.

Sequencing

DNA / RNA were extracted from peripheral blood samples, in the patient also from bone marrow and the fibroblast line (AllPrep DNA/RNA Kit, Qiagen, Hilden, Germany). A 100 bp single-read whole-exome sequencing run was performed on an Illumina HiSeq2000 platform (Illumina, San Diego, CA, USA) running on HiSeq control software (HCS) 1.4.8. For library preparation and recovery of captured DNA, sample preparation was carried out using the NimbleGen SeqCapEZ2.0 (Roche NimbleGen, Madison, WI, US). Cluster generation was performed with Truseq SR Cluster kit v3 (Illumina) and sequencing run was executed using Truseq SBS kit v3-HS (Illumina). Raw image data conversion was performed using consensus assessment of sequence and variation version 1.8.2 (CASAVA). Reads were aligned to the reference genome (hg19/grch37) using BWA and alignment post-processing was carried out

with SAM- and Picard-tools. Called and filtered SNVs were annotated with the Variant Effect Predictor (VEP) from Ensembl using the local copy of Ensembl database (Ensembl 70 and dbSNP137) as well as the prediction tools SIFT and Polyphen. Annotated SNVs were uploaded into an internal SQL database. Quality scores of the called SNVs were set with a Phred-like Score of min. 30 and sequencing reached a 30x coverage for ≥80% of targeted regions in average. Common variants, defined as those present in dbSNP137 with a minor allele frequency ≥ 15%, were filtered out. Interactions with genes of known primary immunodeficiencies and DNA repair disorders were visualized by in-house programming based on STRING-DB9. Found mutations were confirmed by capillary sequencing. RAD52 mRNA expression was analyzed by Real Time PCR with an ABI PRISM 7900HT (Applied Biosystems, Foster City, CA, USA)

Electrophoretic Mobility Shift Assay (EMSA)

We assayed the ability of wt and mutant protein to bind DNA by performing EMSA as previously described [1]. Briefly, we preincubated 0,1 µL of 10 µM 32P-labeled 5S-repeat oligonucleotide (eurofins genomics, Ebersberg, Germany) with 2 µL buffer D at 37°C for 5 min. Subsequently, different concentrations (0-1 µM) of wt RAD52 and P183S RAD52 protein (OriGene, Rockville, MD, USA) were added and incubated for 5 min. Complexes were then fixed with 1% glutaraldehyde at 37°C for 20 min and fractionated through a 4% polyacrylamide gel in 0.25x TBE buffer for 1 h at 250 V. Gels were dried, exposed to an imaging plate, and visualized using FLA-7000 (FUJIFILM Life Science, Stamford, CT, USA). Densitometry was performed using LAS-3000 software.

Structural modeling

Molecular dynamics simulations

The starting structure for human RAD52 wt was taken from the *apo* crystal structure of the undecamer (PDB ID 1KN0). The P183S variant was generated therefrom by removing side chain atoms of proline and adding those of serine with the help of the program leap from the AMBER 10 suite of programs. For the MD simulations, the ff99SB force field was used for the protein. Each protein structure was placed into an octahedral periodic box of TIP3P water molecules, with distances between the edges of the water box and the closest atom of the protein of at least 11 Å. The particle mesh Ewald method was used to treat long-range electrostatic interactions. Bond lengths involving bonds to hydrogen atoms were constrained using SHAKE. The time-step for all MD simulations was 2 fs, with a direct-space, non-bonded cutoff of 8 Å. Applying harmonic restraints with force constants of 5 kcal mol^{-1} $Å^{-2}$ to all solute atoms, NVT-MD was carried out for 50 ps, during which the system was heated from 100 K to 300 K. Subsequent NPT-MD was used for 150 ps to adjust the solvent density. Finally, the force constants of the harmonic restraints on solute atom positions were gradually reduced to zero during 100 ps of NVT-MD. The following 80 ns of NVT-MD at 300 K were used for analysis with the program ptraj, with conformations extracted every 20 ps. Independent duplicate MD simulations were performed to test for the robustness of the results. No gross differences were observed with respect to structural deviations across the two MD simulations, respectively, for RAD52 wt and the P183S variant (Figure S6).

Foci formation

HT-1080 cells were stably transfected with wt EGFP-RAD52 and EGFP-RAD52^{P183S} via bicistronic expression vectors previously used for stable expression in human cells [2]. Cells were seeded at a density of 4000 cells/cm^2 and irradiated one day later with a calibrated X-ray source (Xstrahl RS225, Gulmay Medical, Camberley, UK) at a dose rate of 1 or 10 Gy /min. Subsequently the cell line was cultured for 4 or 24 hours respectively and analyzed by phase contrast and epifluorescence microscopy on a Zeiss Axiovert 100 (Carl Zeiss, Oberkochen, Germany) inverted light microscope equipped with an on-stage heating chamber (TC3 from Bioptechs, Butler, PA, USA), a heated 63×/1.4NA oil immersion objective system, a mercury lamp and appropriate filter sets.

Results

Polyphen2 result of P183S variant

Possibly damaging with a score of **0.839** (sensitivity: **0.84**; specificity: **0.93**)

Molecular dynamics simulations of RAD52 wt and the P183S variant

All-atom MD simulations of undecameric RAD52 wt and the P183S variant of 80 ns length were performed. Average structures of both protein variants are highly structurally similar (C_α atom root mean square deviation: 1.0 Å; Figure 1A, B), indicating only a local influence of the P183S mutation. Analysis of root mean square fluctuations of atomic coordinates confirmed this result, showing differences in atomic mobility between wt and the P183S variant predominantly

in the loop between helices α4 and α5, the location of the mutation (Figure 1C), in helix α4 itself, and the preceding region of 3_{10} helices (Figure S7A). Notably, the P183S mutations stabilizes these structural elements, as shown by a decrease of atomic mobility compared to wt (Figure S7A). The stabilization is accompanied by a tighter packing between S183 and helix α4' of the neighboring protomer, as demonstrated by more frequent short distances between the C_α atom of S183 and the center of α4' than between P183 and α4' (Figure 75B). Investigating interactions formed by S183 to identify the origin of this stabilization revealed that the side chain of S183 temporarily interacts with the sidechain of K169 by a charge-assisted hydrogen bond (distance between the two polar sidechain atoms as close as 3 Å; Figure S7C); such an interaction is precluded for proline. As a consequence, the sidechain of K169 points for about half of the time towards S183 and, hence, to the outside of the undecamer (Figure S7D). In contrast, in the wt, the sidechain is predominantly oriented towards the center (Figure S7D), placing its positive charge close to the implicated ssDNA binding grove (Figure 1C) [3, 4]. We thus hypothesized that the reorientation of K169, triggered by the P183S mutation, disturbs ssDNA binding and, hence, the ssDNA annealing function of RAD52.

Foci formation:

10 Gy, 4h: 32 cells with 1033 foci in wt and 31 cells with 882 foci in P183S were counted (p=0.5)

10 Gy, 24h: 13 cells with 368 Foci in wt and 10 cells with 196 foci in P183S were counter (p=0.29)

Supplemental figures

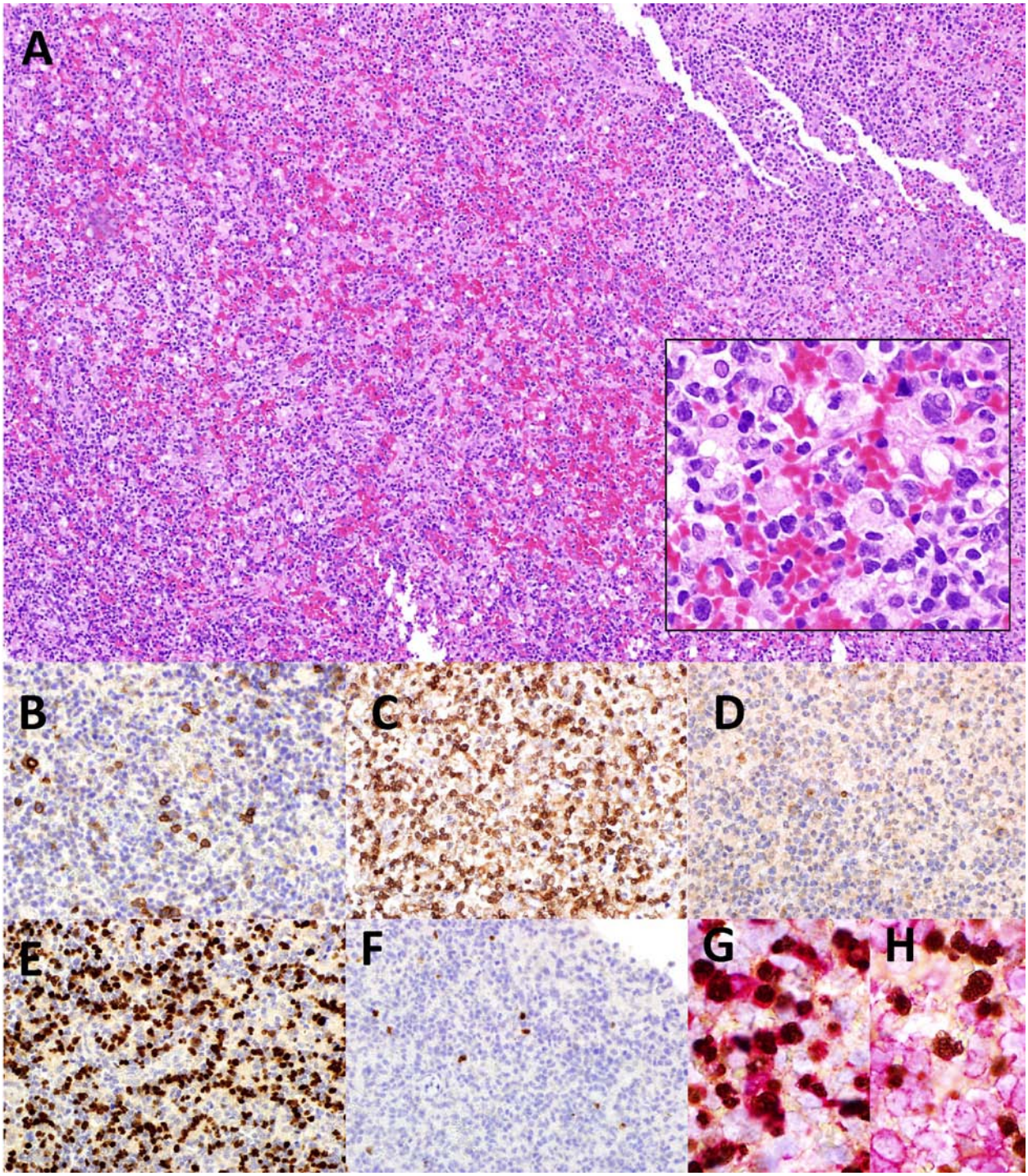

Figure S1 - Lymph node biopsy with complete effacement of the architecture and a polymoprhic infiltrate composed of lymphocytes, histiocytes and blastic cells (A, hematoxylin and eosin). The number of CD20 positive B-cells is reduced (B) and among the T-cells α/β T-cells (TCRβ chain, C) are dominating over γ/δ T-cells (TCRγ chain, D). Most blastic cells harbor EBV (EBER in situ hybridization, E) and some of these cells express EBNA2 (F) indicating a latency type III. Double staining for CD79a (red) and EBER (brown) suggests that most EBV-positive cells are B-cells (G) rather than T-cells (CD3 red and EBER brown, H).

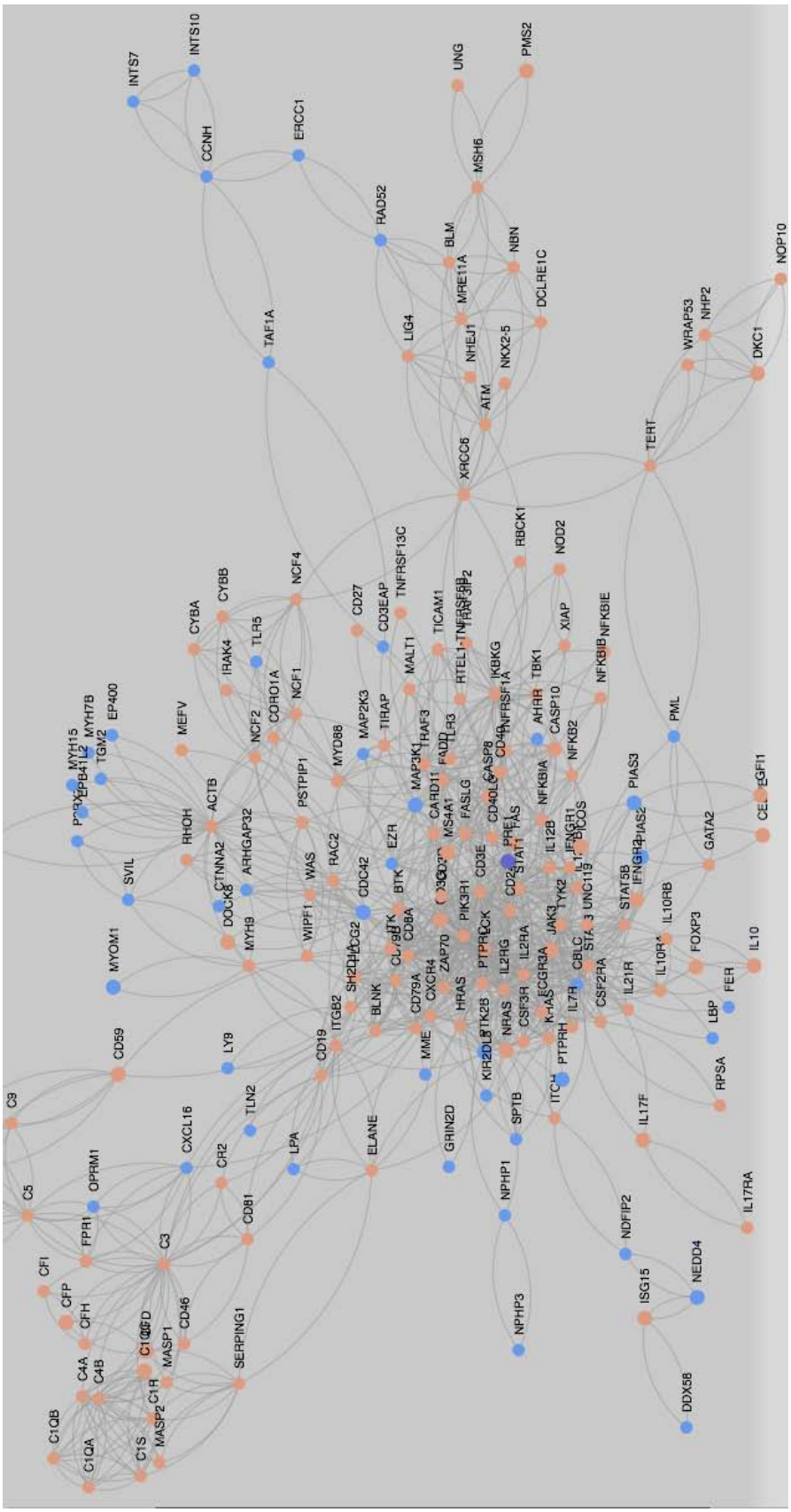
INTS7
INTS10
CCNH
ERCC1
RAD52
UNG
PMS2
MSH6
BLM
MRE11A
NBN
DCLRE1C
NOP10
NHP2
WRAP53
DKC1
TAF1A
LIG4
NHEJ1
NKX2-5
ATM
XRCC6
TERT
RBCK1
NOD2
NCF4
CD27
CD3EAP
TNFRSF13C
CYBA
CYBB
TLR5
IRAK4
TICAM1
MALT1
IKBKG
NFKBIB
NFKBIE
XIAP
TBK1
AHR
CASP10
NFKB2
NFKBIA
PML
PIAS3
PIAS2
CEBPG
GFI1
GATA2
IL10RB
IL10R
FOXP3
IL10
FER
LBP
RPSA
IL17F
IL17RA
NDFIP2
NEDD4
ISG15
DDX58
NPHP3
NPHP1
SPTB
ITCH
PTPRH
KIR2DL3
GRIN2D
ELANE
LPA
TLN2
LY9
CD19
CD59
MYOM1
SVIL
RHOH
ACTB
CTNNA2
DOCK8
MYH9
ARHGAP32
WIPF1
WAS
RAC2
CDC42
ITGB2
SH2D1A
BLNK
CD79A
CXCR4
HRAS
NRAS
CSF3R
KRAS
IL7R
CSF2RA
IL21R
IL2RG
IL2RA
JAK3
TYK2
STAT5B
STAT1
IFNGR2
IFNGR1
IL12B
ZAP70
PTPRC
LCK
CD3E
PRF1
FAS
FASLG
CD40LG
CD40
CD8A
PIK3R1
BTK
EZH
MS4A1
CARD11
MAP3K1
IRAF3
FADD
TLR3
RTEL1-TNFRSF6B
TNFRSF1A
TIRAP
MAP2K3
MYD88
PSTPIP1
NCF1
CORO1A
NCF2
MEFV
EP400
TGM2
EPB41L2
MYH15
MYH7B
P3[illegible]
C9
C5
CFI
CFP
CFH
C4A
C4B
C1QB
C1QA
C1S
C1R
MASP2
MASP1
CD46
SERPING1
C3
FPR1
OPRM1
CXCL16
CR2
CD81

Figure S2 - Gene-association network of genes involved in primary immunodeficiencies (PID) as defined by IUIS and further reported in literature (Tab. S1 and [5]). Orange dots represent PID genes without detected SNVs; violet dots represent PID genes with found SNV; blue dots represent found SNV in genes which are directly or indirectly connected to known PID genes. RAD52 has been found in interaction with genes, that give rise to PIDs with DNA repair defect; furthermore, it is the only gene showing a heterozygous phenotype in the patient and his mother.

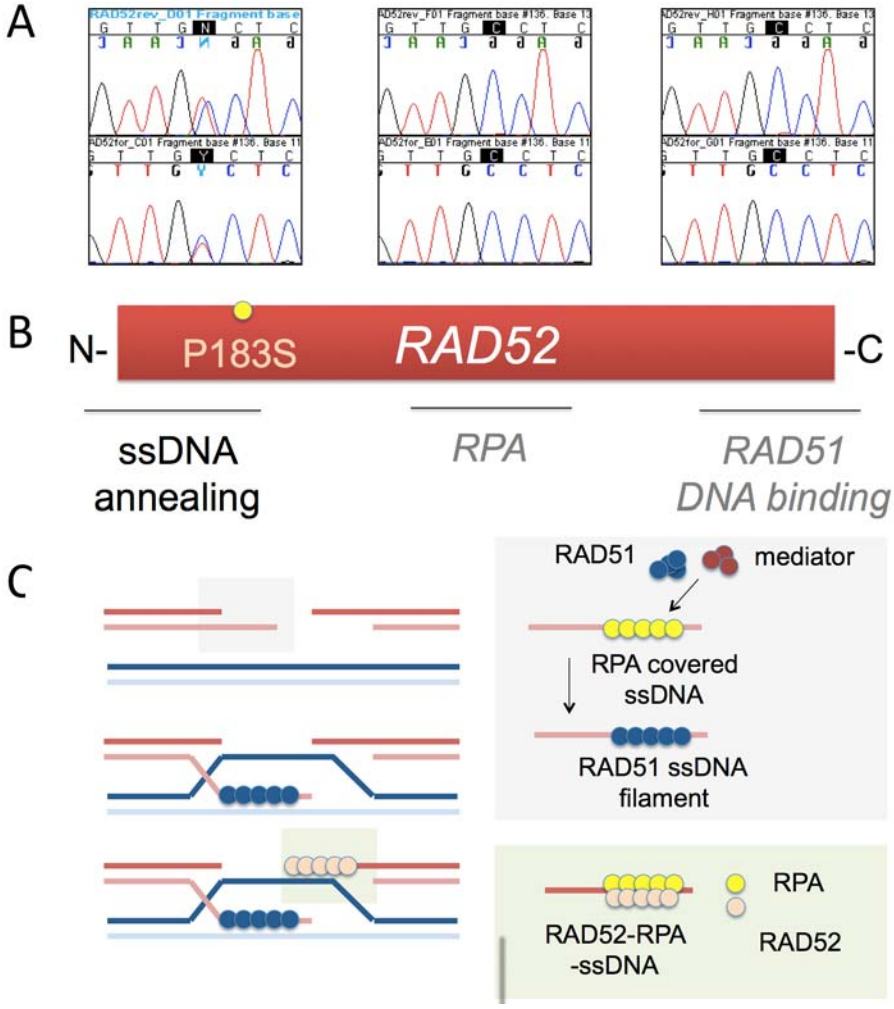
A
B
N-
P183S
RAD52
-C
ssDNA
annealing
RPA
RAD51
DNA binding
C
RAD51
mediator
RPA covered
ssDNA
RAD51 ssDNA
filament
RPA
RAD52
RAD52-RPA
-ssDNA

Figure S3 - (A) Capillary sequencing of RAD52 showing the heterozygous c.547C>T variant in the patient (left) and wt sequence in father (middle) and sister (right). The mother has the same phenotype as the patient. Sequence given with reverse (top graph) and forward primer (bottom graph) applied. (B) Domain organization of the RAD52 protein. While the N-terminal ssDNA annealing site has been studied in depth in human, the mediating function of RAD52 for RAD51 activity (through RPA and the RAD51 binding site) is still debated. (C) Homologous recombination (HR) is a key DNA repair pathway for double strand breaks (DSB) and interstrand cross links (ICL). 1) RAD51 recombinase filament needed for strand invasion into a homologous sequence. In *S. cerevisiae* RAD52 mediates this step; in human, most probably BRCA2 and other proteins can mediate it as well. 2) Strand invasion into a homologous sequence with D-loop formation. 3) After capture of the second end of the DSB and strand extension RAD52 anneals RPA-coated ssDNA (Model based on [6]).

Figure S4 - Skin manifestations of T cell depletion in the patient. Left and middle: Severe zoster infection with VZV in the left ear lobe and lower left leg with necrotizing skin affection. Middle and right: Lower extremities showing widespread vasculitis-like lesions, possibly as sign of dysregulation.

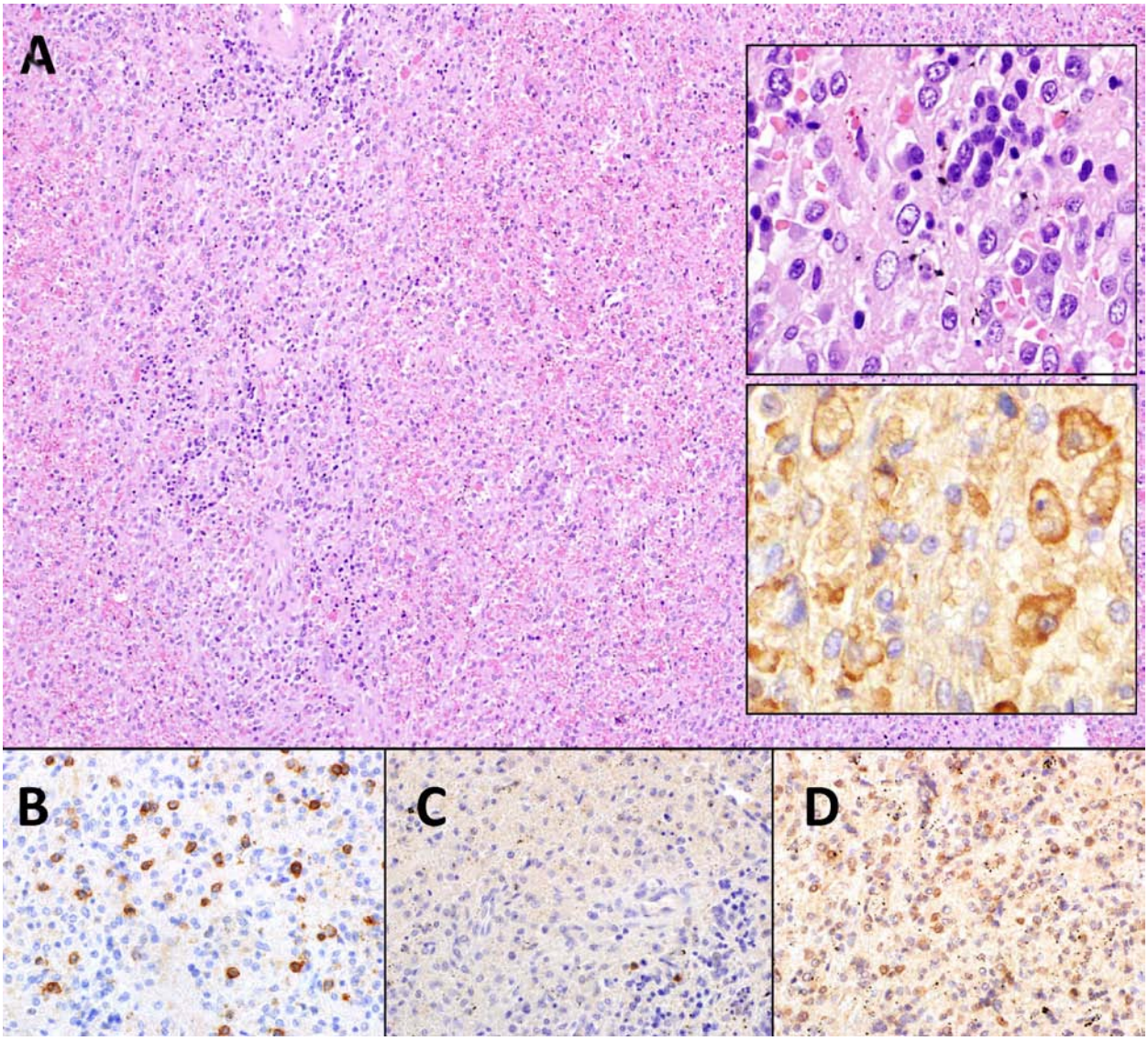

Figure S5 - Splenic tissue with strongly reduced white pulp (A, hematoxylin and eosion), extramedullary hematopoiesis (upper insert in A, hematoxylin and eosin) and increased hemophagocytosis (lower insert in A, CD163). The spleen is depleted of lymphatic cells but among T-cells (CD3, B) α/β T-cells are in minority (TCRβ chain, C) compared to γ/δ T-cells (TCRγ chain, D).

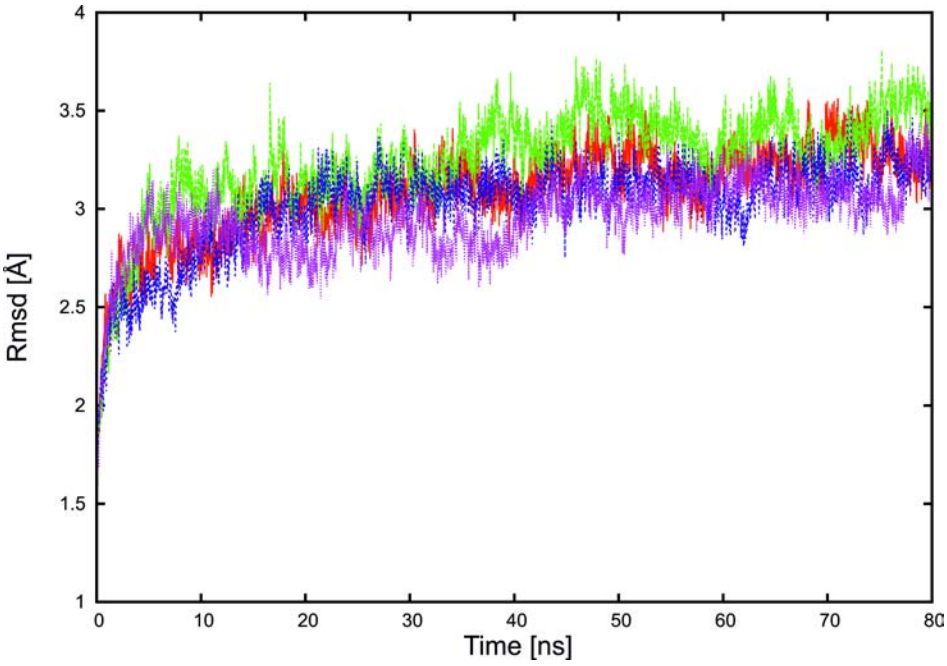

Figure S6 - Structural deviation over the course of the MD simulations. The Cα atom rmsd with respect to the starting structures is depicted for two independent MD simulations each of RAD52 wt (red, green) and the P183S variant (blue, magenta).

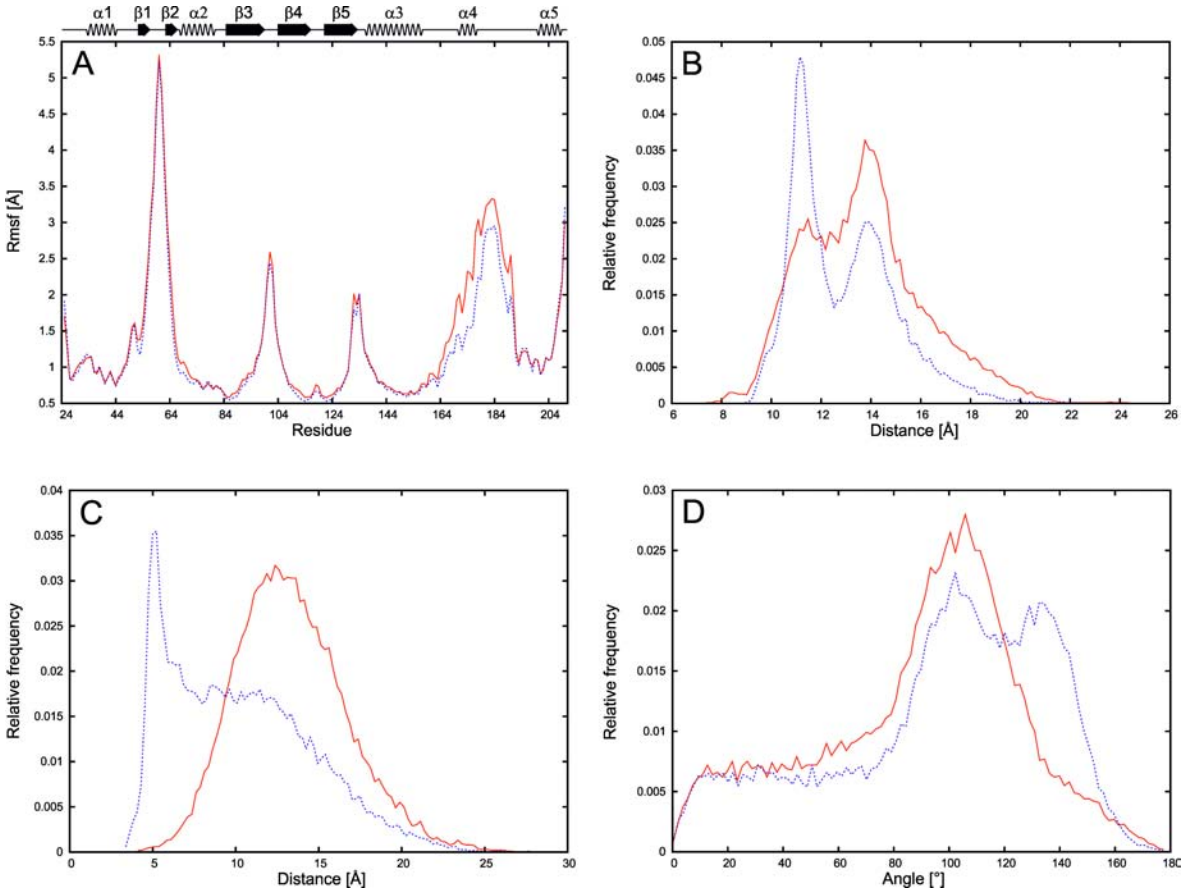

Figure S7 - Local influence of the P183S mutation on dynamics and structure. (A) Rmsf of C_α atoms determined from the MD simulations of wt (red) and mutant (blue) RAD52. The values were averaged over the 11 protomers. The secondary structure of a protomer is depicted at the top of the plot. **(B)** Frequency distribution of the distance between the C_α atom of residue 183 and the center of α4' for wt (red) and mutant (blue). The distributions comprise values of all 11 protomers. **(C)** Frequency distribution of the distance between C_γ of P183 (red) or O_γ of S183 (blue) and N_z of K169, respectively. The distributions comprise values of all 11 protomers. **(D)** Frequency distribution of the angle defined by the point tripe (C_ε of K169; N_z of K169; center of the 11mer) for wt (red) and mutant (blue). The distributions comprise values of all 11

protomers. Angle values closer to 0 indicate an orientation of the side chain of K169 towards the center; angle values closer to 180° indicate an orientation pointing to the outside of the 11mer.

Table S1 (see file) - Tab WES results: Whole-exome sequencing results detecting 129 intragenic non-synonymous single-nucleotide-variants, which are shared by patient and his mother, which are not reported in public databases (HapMap, 1000 Genomes) and have a GMAF of less than 15%.

Tab PID genes: 265 genes reported by IUIS and literature to be causative in primary immunodeficiency disorders.

References

1. Kagawa W, Kagawa A, Saito K, et al. Identification of a second DNA binding site in the human Rad52 protein. J Biol Chem. 2008;283(35):24264-24273.

2. Linka RM, Risse SL, Bienemann K, et al. Loss-of-function mutations within the IL-2 inducible kinase ITK in patients with EBV-associated lymphoproliferative diseases. Leukemia. 2012;26(5):963-971.

3. Kagawa W, Kurumizaka H, Ishitani R, et al. Crystal structure of the homologous-pairing domain from the human Rad52 recombinase in the undecameric form. Mol Cell. 2002;10(2):359-371.

4. Singleton MR, Wentzell LM, Liu Y, West SC, Wigley DB. Structure of the single-strand annealing domain of human RAD52 protein. Proc Natl Acad Sci U S A. 2002;99(21):13492-13497.

5. Bousfiha A, Jeddane L, Al-Herz W, et al. The 2015 IUIS Phenotypic Classification for Primary Immunodeficiencies. J Clin Immunol. 2015;35(8):727-738.

6. Liu J, Heyer WD. Who's who in human recombination: BRCA2 and RAD52. Proc Natl Acad Sci U S A. 2011;108(2):441-442.

superregion	regions.name	regions.start	regions.stop
'1:897009-897009'	'1'	'897009'	'897009'
'1:906769-906769'	'1'	'906769'	'906769'
'1:1416235-1416238'	'1'	'1416235'	'1416238'
'1:1688096-1688096'	'1'	'1688096'	'1688096'
'1:1920434-1920435'	'1'	'1920434'	'1920435'
'1:22405202-22405202'	'1'	'22405202'	'22405202'
'1:60073550-60073550'	'1'	'60073550'	'60073550'
'1:65099699-65099702'	'1'	'65099699'	'65099700'
'1:65099699-65099702'	'1'	'65099700'	'65099702'
'1:67558869-67558874'	'1'	'67558869'	'67558874'
'1:78958893-78958893'	'1'	'78958893'	'78958893'
'1:85733737-85733742'	'1'	'85733737'	'85733742'
'1:92637073-92637076'	'1'	'92637073'	'92637076'
'1:108690920-108690920'	'1'	'108690920'	'108690920'
'1:109805583-109805583'	'1'	'109805583'	'109805583'
'1:110923619-110923619'	'1'	'110923619'	'110923619'
'1:117633372-117633373'	'1'	'117633372'	'117633373'
'1:145586839-145586839'	'1'	'145586839'	'145586839'
'1:166818273-166818273'	'1'	'166818273'	'166818273'
'1:166961911-166961912'	'1'	'166961911'	'166961912'
'2:28808668-28808668'	'2'	'28808668'	'28808668'
'2:43624982-43624983'	'2'	'43624982'	'43624983'
'2:48732824-48732827'	'2'	'48732824'	'48732827'
'2:73476417-73476418'	'2'	'73476417'	'73476418'
'2:110959026-110959026'	'2'	'110959026'	'110959026'
'2:113940062-113940062'	'2'	'113940062'	'113940062'
'2:197729945-197729946'	'2'	'197729945'	'197729946'
'2:242189205-242189207'	'2'	'242189205'	'242189207'
'3:128695828-128695828'	'3'	'128695828'	'128695828'
'3:132295797-132295797'	'3'	'132295797'	'132295797'
'3:133305986-133305989'	'3'	'133305986'	'133305989'
'3:135870104-135870104'	'3'	'135870104'	'135870104'
'3:141163362-141163362'	'3'	'141163362'	'141163362'
'3:155649576-155649576'	'3'	'155649576'	'155649576'
'3:158422727-158422728'	'3'	'158422727'	'158422728'
'4:265547-265547'	'4'	'265547'	'265547'
'4:5528115-5528116'	'4'	'5528115'	'5528116'
'4:39471680-39471680'	'4'	'39471680'	'39471680'
'4:62936092-62936092'	'4'	'62936092'	'62936092'
'5:434284-434284'	'5'	'434284'	'434284'
'5:31532534-31532534'	'5'	'31532534'	'31532534'
'5:40843735-40843735'	'5'	'40843735'	'40843735'
'5:178413123-178413123'	'5'	'178413123'	'178413123'
'6:123126106-123126106'	'6'	'123126106'	'123126106'
'6:128134516-128134516'	'6'	'128134516'	'128134516'

'6:132891675-132891675'	'6'	'132891675'	'132891675'
'6:151907027-151907027'	'6'	'151907027'	'151907027'
'6:154428919-154428919'	'6'	'154428919'	'154428919'
'6:158612965-158612966'	'6'	'158612965'	'158612966'
'7:6641927-6641930'	'7'	'6641927'	'6641930'
'7:92140455-92140456'	'7'	'92140455'	'92140456'
'7:158683974-158683974'	'7'	'158683974'	'158683974'
'8:19681436-19681436'	'8'	'19681436'	'19681436'
'8:21956096-21956096'	'8'	'21956096'	'21956096'
'8:27668091-27668094'	'8'	'27668091'	'27668094'
'8:38693699-38693699'	'8'	'38693699'	'38693699'
'8:61757805-61757805'	'8'	'61757805'	'61757805'
'8:80976814-80976814'	'8'	'80976814'	'80976814'
'8:133076288-133076289'	'8'	'133076288'	'133076289'
'8:133807184-133807188'	'8'	'133807184'	'133807188'
'9:97349591-97349591'	'9'	'97349591'	'97349591'
'10:70951397-70951401'	'10'	'70951397'	'70951401'
'10:71010270-71010272'	'10'	'71010270'	'71010272'
'10:72360387-72360387'	'10'	'72360387'	'72360387'
'10:135123729-135123729'	'10'	'135123729'	'135123729'
'11:7689029-7689029'	'11'	'7689029'	'7689029'
'11:20658776-20658776'	'11'	'20658776'	'20658776'
'11:28116352-28116352'	'11'	'28116352'	'28116352'
'11:115109386-115109388'	'11'	'115109386'	'115109388'
12:1025983-1025983'	'12'	1025983'	'1025983'
'12:1906632-1906632'	'12'	'1906632'	'1906632'
'12:44131973-44131975'	'12'	'44131973'	'44131975'
'12:102040416-102040417'	'12'	'102040416'	'102040417'
'12:120750398-120750398'	'12'	'120750398'	'120750398'
'12:125299542-125299542'	'12'	'125299542'	'125299542'
'12:133351746-133351746'	'12'	'133351746'	'133351746'
'13:20579458-20579460'	'13'	'20579458'	'20579460'
'13:21142007-21142008'	'13'	'21142007'	'21142008'
'13:21955635-21955635'	'13'	'21955635'	'21955635'
'13:23929941-23929941'	'13'	'23929941'	'23929941'
'13:25828007-25828007'	'13'	'25828007'	'25828007'
'13:25905482-25905486'	'13'	'25905482'	'25905486'
'13:36748957-36748957'	'13'	'36748957'	'36748957'
'13:98896944-98896944'	'13'	'98896944'	'98896944'
'14:58899156-58899157'	'14'	'58899156'	'58899157'
'14:60585287-60585287'	'14'	'60585287'	'60585287'
'14:65209817-65209817'	'14'	'65209817'	'65209817'
'14:89206861-89206861'	'14'	'89206861'	'89206861'
'14:94750336-94750336'	'14'	'94750336'	'94750336'
'14:95660243-95660243'	'14'	'95660243'	'95660243'
'15:38990475-38990475'	'15'	'38990475'	'38990475'

'15:40707595-40707595'	'15'	'40707595'	'40707595'
'15:41247859-41247859'	'15'	'41247859'	'41247859'
'15:41339697-41339697'	'15'	'41339697'	'41339697'
'15:65684513-65684513'	'15'	'65684513'	'65684513'
'15:66840941-66840941'	'15'	'66840941'	'66840941'
'15:67692566-67692566'	'15'	'67692566'	'67692566'
'15:67786675-67786675'	'15'	'67786675'	'67786675'
'15:78454050-78454050'	'15'	'78454050'	'78454050'
'15:78880752-78880752'	'15'	'78880752'	'78880752'
'16:87377375-87377378'	'16'	'87377375'	'87377378'
'17:1678517-1678518'	'17'	'1678517'	'1678518'
'17:2139741-2139745'	'17'	'2139741'	'2139745'
'17:3352438-3352438'	'17'	'3352438'	'3352438'
'17:3635804-3635805'	'17'	'3635804'	'3635805'
'17:5336215-5336216'	'17'	'5336215'	'5336216'
'17:5351995-5351998'	'17'	'5351995'	'5351998'
'17:21205561-21205561'	'17'	'21205561'	'21205561'
'17:77921593-77921593'	'17'	'77921593'	'77921593'
'18:24497190-24497190'	'18'	'24497190'	'24497190'
'18:44392443-44392443'	'18'	'44392443'	'44392443'
'19:868897-868897'	'19'	'868897'	'868897'
'19:2273082-2273082'	'19'	'2273082'	'2273082'
'19:41518573-41518573'	'19'	'41518573'	'41518573'
'19:42907004-42907004'	'19'	'42907004'	'42907004'
'19:44660791-44660791'	'19'	'44660791'	'44660791'
'19:46305530-46305530'	'19'	'46305530'	'46305530'
'19:47884089-47884089'	'19'	'47884089'	'47884089'
'19:48259029-48259029'	'19'	'48259029'	'48259029'
'19:55450727-55450727'	'19'	'55450727'	'55450727'
'19:57724072-57724072'	'19'	'57724072'	'57724072'
'20:19654276-19654276'	'20'	'19654276'	'19654276'
'20:33588590-33588591'	'20'	'33588590'	'33588591'
'20:35675512-35675512'	'20'	'35675512'	'35675512'
'20:36643159-36643161'	'20'	'36643159'	'36643161'
'20:36932647-36932647'	'20'	'36932647'	'36932647'
'22:41190621-41190622'	'22'	'41190621'	'41190622'
'22:44681317-44681317'	'22'	'44681317'	'44681317'
'X:7811713-7811713'	'X'	'7811713'	'7811713'

alterations.ref	alterations.alt	genetic_elements.ensembl_gene_id	genetic_elements.hgnc
'A'	'G'	ENSG00000187961'	'KLHL17'
'C'	'A'	ENSG00000187583'	'PLEKHN1'
'GCTT'	'G'	'ENSG00000160072'	'ATAD3B'
'C'	'T'	'ENSG00000008130'	'NADK'
'T'	'TA'	'ENSG00000142609'	'C1orf222'
'T'	'A'	'ENSG00000070831'	'CDC42'
'A'	'C'	'ENSG00000172456'	'FGGY'
'TG'	'T'	'ENSG00000158966'	'CACHD1'
'GGT'	'G'	'ENSG00000158966'	'CACHD1'
'CTCATT'	'C'	'ENSG00000203963'	'C1orf141'
'G'	'A'	'ENSG00000122420'	'PTGFR'
'TGTTAA'	'T'	'ENSG00000142867'	'BCL10'
'CTTA'	'C'	'ENSG00000069712'	'KIAA1107'
'G'	'A'	'ENSG00000085491'	'SLC25A24'
'C'	'A'	'ENSG00000143126'	'CELSR2'
'G'	'T'	'ENSG00000168679'	'SLC16A4'
'C'	'CT'	'ENSG00000116830'	'TTF2'
'C'	'T'	'ENSG00000186364'	'NUDT17'
'C'	'T'	'ENSG00000143157'	'POGK'
'AT'	'A'	'ENSG00000143194'	'MAEL'
'A'	'G'	'ENSG00000163803'	'PLB1'
'GA'	'G'	'ENSG00000115970'	'THADA'
'ATTG'	'A'	'ENSG00000162869'	'PPP1R21'
'G'	'GT'	'ENSG00000135624'	'CCT7'
'G'	'T'	'ENSG00000144061'	'NPHP1'
'A'	'G'	'ENSG00000125637'	'PSD4'
'TA'	'T'	'ENSG00000197121'	'PGAP1'
'CAA'	'C'	'ENSG00000115677'	'HDLBP'
'G'	'A'	'ENSG00000114656'	'KIAA1257'
'G'	'C'	'ENSG00000240303'	'ACAD11'
'AAAT'	'A'	'ENSG00000091527'	'CDV3'
'C'	'T'	'ENSG00000174579'	'MSL2'
'G'	'T'	'ENSG00000177311'	'ZBTB38'
'A'	'C'	'ENSG00000163655'	'GMPS'
'CA'	'C'	'ENSG00000118849'	'RARRES1'
'A'	'G'	'ENSG00000186777'	'ZNF732'
'AT'	'A'	'ENSG00000082929'	'C4orf6'
'G'	'A'	'ENSG00000121897'	'LIAS'
'C'	'A'	'ENSG00000150471'	'LPHN3'
'C'	'T'	'ENSG00000063438'	'AHRR'
'G'	'C'	'ENSG00000082213'	'C5orf22'
'C'	'A'	'ENSG00000132357'	'CARD6'
'G'	'A'	'ENSG00000113262'	'GRM6'
'T'	'G'	'ENSG00000172594'	'SMPDL3A'
'C'	'T'	'ENSG00000172673'	'THEMIS'

'C'	'T'	'ENSG00000146383'	'TAAR6'
'G'	'A'	'ENSG00000120262'	'CCDC170'
'G'	'A'	'ENSG00000112038'	'OPRM1'
'AT'	'A'	'ENSG00000185068'	'GTF2H5'
'CAAG'	'C'	'ENSG00000146576'	'C7orf26'
'CT'	'C'	'ENSG00000127980'	'PEX1'
'T'	'G'	'ENSG00000126870'	WDR60'
'G'	'T'	'ENSG00000104613'	'INTS10'
'G'	'A'	'ENSG00000158863'	'FAM160B2'
'TCTC'	'T'	'ENSG00000168078	ENSG00000171320'
'C'	'T'	'ENSG00000147526'	'TACC1'
'C'	'T'	'ENSG00000171316'	'CHD7'
'C'	'A'	'ENSG00000076554'	'TPD52'
'G'	'GA'	'ENSG00000258417	ENSG00000132297'
'GTATT'	'G'	'ENSG00000129292'	'PHF20L1'
'G'	'T'	'ENSG00000130957'	'FBP2'
'TTCTG'	'T'	'ENSG00000156502'	'SUPV3L1'
'GCT'	'G'	'ENSG00000156510'	'HKDC1'
'G'	'A'	'ENSG00000180644'	'PRF1'
'A'	'G'	'ENSG00000198546'	'ZNF511'
'A'	'C'	'ENSG00000166394'	'CYB5R2'
'G'	'T'	'ENSG00000165970'	'SLC6A5'
'G'	'A'	'ENSG00000121621'	'KIF18A'
'CAG'	'C'	'ENSG00000182985'	'CADM1'
'G'	'A'	'ENSG00000002016'	'RAD52'
'G'	'A'	'ENSG00000151062'	'CACNA2D4'
'TAA'	'T'	'ENSG00000129317	ENSG00000257896'
'C'	'CA'	'ENSG00000196091'	'MYBPC1'
'C'	'T'	'ENSG00000089163'	'SIRT4'
'C'	'T'	'ENSG00000073060'	'SCARB1'
'C'	'T'	'ENSG00000090615'	'GOLGA3'
'CTT'	'C'	'ENSG00000121741'	'ZMYM2'
'G'	'GT'	'ENSG00000032742'	'IFT88'
'C'	'T'	'ENSG00000180776'	'ZDHHC20'
'A'	'C'	'ENSG00000151835'	'SACS'
'G'	'T'	'ENSG00000139505'	'MTMR6'
'A'	'ATTTT'	'ENSG00000139496'	'NUPL1'
'C'	'T'	'ENSG00000120669	ENSG00000250709'
'A'	'G'	'ENSG00000152767'	'FARP1'
'AG'	'A'	'ENSG00000100578'	'KIAA0586'
'A'	'G'	'ENSG00000126773'	'PCNXL4'
'C'	'T'	'ENSG00000126822'	'PLEKHG3'
'G'	'A'	'ENSG00000165521'	'EML5'
'A'	'T'	'ENSG00000140093'	'SERPINA10'
'T'	'C'	'ENSG00000165959'	'CLMN'
'C'	'T'	'ENSG00000175779'	'C15orf53'

'G'	'A'	'ENSG00000128928'	'IVD'
'A'	'T'	'ENSG00000128965'	'CHAC1'
'T'	'C'	'ENSG00000128908'	'INO80'
'C'	'T'	'ENSG00000103742'	'IGDCC4'
'G'	'C'	'ENSG00000188501'	'LCTL'
'T'	'C'	'ENSG00000103599'	'IQCH'
'C'	'T'	'ENSG00000103599'	'IQCH'
'T'	'A'	'ENSG00000166411'	'IDH3A'
'G'	'A'	'ENSG00000169684'	'CHRNA5'
'CAGG'	'C'	'ENSG00000103264'	'FBXO31'
'T'	'TG'	'ENSG00000132386'	'SERPINF1'
'CTCTA'	'C'	'ENSG00000070366'	'SMG6'
'C'	'G'	'ENSG00000141255	ENSG00000262314'
'AC'	'A'	'ENSG00000083457'	'ITGAE'
'A'	'AT'	'ENSG00000108561'	'C1QBP'
'CCTT'	'C'	'ENSG00000005100	ENSG00000108561'
'T'	'C'	'ENSG00000034152'	'MAP2K3'
'C'	'T'	'ENSG00000167291'	'TBC1D16'
'C'	'T'	'ENSG00000154080'	'CHST9'
'T'	'C'	'ENSG00000078043'	'PIAS2'
'C'	'T'	'ENSG00000175221'	'MED16'
'A'	'T'	'ENSG00000104904'	'OAZ1'
'C'	'T'	'ENSG00000197408'	'CYP2B6'
'C'	'T'	'ENSG00000079435'	'LIPE'
'G'	'A'	'ENSG00000263002'	'ZNF234'
'T'	'C'	'ENSG00000104941'	'RSPH6A'
'G'	'A'	'ENSG00000134815'	'DHX34'
'A'	'G'	'ENSG00000105373'	'GLTSCR2'
'C'	'T'	'ENSG00000167634'	'NLRP7'
'A'	'C'	'ENSG00000083844'	'ZNF264'
'C'	'G'	'ENSG00000185052'	'SLC24A3'
'AG'	'A'	'ENSG00000078814'	'MYH7B'
'G'	'A'	'ENSG00000080839'	'RBL1'
'CAA'	'C'	'ENSG00000101407'	'TTI1'
'G'	'A'	'ENSG00000101425'	'BPI'
'TA'	'T'	'ENSG00000100372'	'SLC25A17'
'G'	'A'	'ENSG00000138944'	'KIAA1644'
'G'	'A'	'ENSG00000182583'	'VCX'

genetic_elements.ensembl_feature_consequence
'[regulatory_region_variant] ENSR00000528861:(I:
'[regulatory_region_variant] ENSR00000162195:(I:
'[feature_truncation] ENST00000472194:(I:
'[splice_region_variant] ENST00000378625:(I:
'[regulatory_region_variant] ENSR00000529131:(I:
'[missense_variant] ENST00000421089:(I:
'[missense_variant] ENST00000371210:(I:
'[feature_truncation] ENST00000495994:(I:
'[feature_truncation] ENST00000495994:(I:
'[frameshift_variant] ENST00000371007:(I:
'[missense_variant] ENST00000370757:(I:
'[feature_truncation] ENST00000271015:(I:
'[feature_truncation] ENST00000370378:(I:
'[missense_variant] ENST00000565488:(I:
'[missense_variant] ENST00000271332:(I:
'[regulatory_region_variant] ENSR00001039754:(I:
'[feature_elongation] ENST00000369466:(I:
'[missense_variant] ENST00000444015:(I:
'[missense_variant] ENST00000449930:(I:
'[feature_truncation] ENST00000447624:(I:
'[missense_variant] ENST00000327757:(I:
'[feature_truncation] ENST00000330266:(I:
'[feature_truncation] ENST00000416913:(I:
'[feature_elongation] ENST00000473786:(I:
'[missense_variant] ENST00000445609:(I:
'[missense_variant] ENST00000441564:(I:
'[feature_truncation] ENST00000409475:(I:
'[feature_truncation] ENST00000498595:(I:
'[missense_variant] ENST00000515659:(I:
'[missense_variant] ENST00000264990:(I:
'[feature_truncation] ENST00000511392:(I:
'[missense_variant] ENST00000309993:(I:
'[regulatory_region_variant] ENSR00001484302:(I:
'[missense_variant] ENST00000496455:(I:
'[feature_truncation] ENST00000479756:(I:
'[regulatory_region_variant] ENSR00001428670:(I:
'[feature_truncation] ENST00000515342:(I:
'[missense_variant] ENST00000381846:(I:
'[regulatory_region_variant] ENSR00001431605:(I:
'[missense_variant] ENST00000505113:(I:
'[regulatory_region_variant] ENSR00001408162:(I:
'[missense_variant] ENST00000381677:(I:
'[splice_region_variant] ENST00000231188:(I:
'[missense_variant] ENST00000539041:(I:
'[missense_variant] ENST00000368250:(I:

'[missense_variant] ENST00000275198:(I:
'[missense_variant] ENST00000239374:(I:
'[missense_variant] ENST00000414028:(I:
'[feature_truncation] ENST00000438073:(I:
'[regulatory_region_variant] ENSR00000064980:(I:
'[feature_truncation] ENST00000476923:(I:
'[missense_variant] ENST00000444851:(I:
'[missense_variant] ENST00000523846:(I:
'[missense_variant] ENST00000450006:(I:
'1'
'[missense_variant] ENST00000520615:(I:
'[splice_region_variant] ENST00000307121:(I:
'[missense_variant] ENST00000517462:(I:
'1'
'[feature_truncation] ENST00000395383:(I:
'[splice_region_variant] ENST00000375337:(I:
'[feature_truncation] ENST00000478227:(I:
'[feature_truncation] ENST00000486754:(I:
'[missense_variant] ENST00000318971:(I:
'[missense_variant] ENST00000361518:(I:
'[missense_variant] ENST00000299498:(I:
'[missense_variant] ENST00000525748:(I:
'[splice_region_variant] ENST00000263181:(I:
'[feature_truncation] ENST00000452722:(I:
'[missense_variant] ENST00000358495:(I:
'[regulatory_region_variant] ENSR00000425176:(I:
'1'
'[feature_elongation] ENST00000536007:(I:
'[missense_variant] ENST00000202967:(I:
'[missense_variant] ENST00000540495:(I:
'[regulatory_region_variant] ENSR00001468567:(I:
'[feature_truncation] ENST00000456228:(I:
'[regulatory_region_variant] ENSR00000512605:(I:
'[missense_variant] ENST00000382466:(I:
'[missense_variant] ENST00000382292:(I:
'[missense_variant] ENST00000540661:(I:
'[feature_elongation] ENST00000463407:(I:
'1'
'[missense_variant] ENST00000376581:(I:
'[frameshift_variant] ENST00000261244:(I:
'[missense_variant] ENST00000406854:(I:
'[missense_variant] ENST00000247226:(I:
'[missense_variant] ENST00000352093:(I:
'[missense_variant] ENST00000393096:(I:
'[missense_variant] ENST00000298912:(I:
'[missense_variant] ENST00000318792:(I:

'[splice_region_variant] ENST00000560660:(I:
'[initiator_codon_variant] ENST00000487220:(I:
'[missense_variant] ENST00000558357:(I:
'[missense_variant] ENST00000352385:(I:
'[missense_variant] ENST00000341509:(I:
'[regulatory_region_variant] ENSR00000237949:(I:
'[missense_variant] ENST00000546225:(I:
'[missense_variant] ENST00000559881:(I:
'[missense_variant] ENST00000394802:(I:
'[splice_region_variant] ENST00000563113:(I:
'[feature_elongation] ENST00000572048:(I:
'[feature_truncation] ENST00000570659:(I:
'1'
'[regulatory_region_variant] ENSR00001533776:(I:
'[feature_elongation] ENST00000225698:(I:
'1'
'[missense_variant] ENST00000526076:(I:
'[regulatory_region_variant] ENSR00001538551:(I:
'[missense_variant] ENST00000581714:(I:
'[missense_variant] ENST00000585916:(I:
'[missense_variant] ENST00000395808:(I:
'[regulatory_region_variant] ENSR00001014741:(I:
'[splice_region_variant] ENST00000593831:(I:
'[regulatory_region_variant] ENSR00000346885:(I:
'[missense_variant] ENST00000592437:(I:
'[splice_region_variant] ENST00000600188:(I:
'[missense_variant] ENST00000328771:(I:
'[missense_variant] ENST00000594182:(I:
'[missense_variant] ENST00000590030:(I:
'[missense_variant] ENST00000263095:(I:
'[missense_variant] ENST00000328041:(I:
'[regulatory_region_variant] ENSR00000400210:(I:
'[missense_variant] ENST00000373664:(I:
'[feature_truncation] ENST00000373447:(I:
'[missense_variant] ENST00000262865:(I:
'[feature_truncation] ENST00000447566:(I:
'[missense_variant] ENST00000381176:(I:
'[missense_variant] ENST00000341408:(I: